**Rare Metal Materials and Engineering**
Volume 49, Issue 6, June 2020
Available online at www.rmme.ac.cn

Science Press

**Cite this article as:** Rare Metal Materials and Engineering, 2020, 49(6): 1873-1878.

ARTICLE

# Microstructure and Surface Corrosion Behavior of Plasma Welding Area of $Al_3Zr$/Al Matrix In-situ Composites

**Li Hui[1], Xu Pinyi[1], Lu Shengbo[1], Jiao Lei[2]**

*[1] Jiangsu University of Science and Technology, Zhenjiang 212003, China; [2] Jiangsu University, Zhenjiang 212013, China*

**Abstract:** 5 wt% $Al_3Zr$/aluminum matrix composites were taken as the research object, and plasma welding was conducted with Ar gas as ion gas and Al-Ti-B as wire materials. The corrosion polarization curve of weld area in 3.5% NaCl solution was measured by electrochemical comprehensive tester. Scanning electron microscope (SEM) and X-ray diffraction analyzer (XRD) were used to analyze and characterize the microstructure and phase composition of the composite and its weld. The corrosion behavior and corrosion mechanism of $Al_3Zr$/aluminum matrix composites after plasma welding were studied in 3.5% NaCl solution. The SEM analysis results show that through plasma arc welding, a better weld can be obtained. The weld microstructure is mainly composed of $Al_3Ti$ phase and Al matrix, and the $Al_3Ti$ phase is striped and spherical. The electrochemical polarization curves indicate that the corrosion resistance of the materials at the nugget is slightly lower than that of the base metal. The immersion corrosion mechanism of weld is that the $Al_3Ti$ phase and the matrix phase behave as the anode and cathode of a primary cell.

**Key words:** $Al_3Zr$/Al matrix composites; plasma welding; corrosion resistance; corrosion mechanism

Aluminum matrix composites have become the hot materials in the field of materials science in the world because of their excellent physical properties and mechanical properties, and the focus of the research and development of new materials in China in the future. In particular, particle reinforced aluminum matrix composites have the advantages of low cost, isotope, good wear resistance, and high performance and functional equability, so they have broad application prospects in high-tech fields, such as aerospace [1-3]. It has become the mainstream of the research and development of aluminum matrix composites. At present, a lot of research work has been done on the preparation process, plastic forming process and heat treatment process of aluminum matrix composites[4-6]. However, the study of welding process and weld ability of the material lags far behind, so it has become a serious obstacle to the practicability of this kind of material. In this study, $Al_3Zr$/aluminum matrix composite was chosen as base material[7-10]. Al-Ti-B was used as wire material, and plasma arc welding technology was used for welding. The weld ability of $Al_3Zr$/aluminum matrix composites was studied. The corrosion resistance and corrosion mechanism of base metal and weld area were investigated by electrochemical comprehensive experiments and immersion experiments.

## 1 Experimental Materials and Methods

### 1.1 Materials

In-situ reaction method was adopted to fabricate 5 wt% $Al_3Zr$/aluminum matrix composites. The raw material was 6082 aluminum alloy and $K_2ZrF_6$ powder, and the reaction temperature was 780 °C. The quality index of $K_2ZrF_6$ and selected aluminum alloy is shown in Table 1 and Table 2, respectively.

### 1.2 Experimental process and parameters

Mixed salt method in 15 Hz excitation stirring field was

**Table 1 Quality index for $K_2ZrF_6$ (wt%)**

| $K_2ZrF_6$ | $Fe_2O_3$ | $H_2O$ |
|---|---|---|
| ≥99.80 | ≤0.05 | ≤0.15 |

Received date: October 08, 2019
Foundation item: National Natural Science Foundation of China (51605206); Postgraduate Research & Practice Innovation Program of Jiangsu Province (KYCX19_1669); Jiangsu Province Key Laboratory of High-end Structural Materials (hsm1806)
Corresponding author: Li Hui, Ph. D., Associate Professor, School of Materials Science and Engineering, Jiangsu University of Science and Technology, Zhenjiang 212003, P. R. China, Tel: 0086-511-84426291, E-mail: lihuiwind@163.com

**Table 2 Chemical composition of aluminum alloy (wt%)**

| Mg | Si | Mn | Fe | Cr | Zn | Cu | Ti | Al |
|---|---|---|---|---|---|---|---|---|
| 0.6~1.2 | 0.7~1.3 | 0.4~1.0 | 0.5 | 0.2 | 0.2 | 0.1 | 0.1 | Bal. |

used to fabricate $Al_3Zr$/aluminum matrix composites. 5 wt% $Al_3Zr$/aluminum matrix composites were processed into 120 mm×50 mm×10 mm sheet by wire cutting. The surface oxide was scrubbed with sandpaper and cleaned with anhydrous alcohol. Then check the water system of the plasma arc welding machine, switch on the power supply, open the Ar cylinder and check the gas system, and adjust the electrode to be coaxial with the nozzle. Adjust the distance between the nozzle and the work-piece, set 2 mm in tungsten electrode and 7 mm in welding torch height; open the micro-arc, 15 s later lead the main arc, and carry on the plasma welding. The parameters of plasma arc welding are as follows: welding speed is 200 mm/min, ion gas flow rate is 1.6 L/min, and welding current is 130 A. During the welding process, the welding pool was aligned with the XVC-1100 welding camera and the whole welding process was recorded. After welding, the power supply was cut off, the ion gas was turned off, the protective gas was closed after 15 s, and the circulating water tank was finally closed. The welded material was cut into 10 mm×10 mm×3 mm for electrochemical test and corrosion test. Microhardness of welded joints was tested by KB30S Vickers hardness tester, and the interval was 0.5 mm.

Corrosion electrochemical experiment was carried out on the Corr-test CS2350 electrochemical workstation. The experimental medium was distilled water and 3.5% NaCl solution prepared with NaCl (analytical purity). The auxiliary electrode for electrochemical measurement was Pt electrode, the reference electrode was saturated calomel electrode, and the working electrode area was 0.9 $cm^2$. When testing the polarization curve, it was started at 500 mV below the corrosion potential, and the scan rate was 1 mV/s, and the current density was $10^{-2}$ $A{\cdot}cm^{-2}$. The scanning frequency was 10 mHz~10 kHz and the sinusoidal signal amplitude was 10 mV.

The saline immersion test was carried out according to GB10124-88, and the dipping medium was 3.5% NaCl solution. During immersion, the solution temperature was controlled at 24±1 °C and the soaking time was 14 d. At the 14th day, the surface soluble impurities were removed by ultrasonic cleaning for 10 min, the surface soluble impurities were cleaned by distilled water, and the microscopic morphology of corrosion was observed by scanning electron microscope (SEM); the saline immersion corrosion products were analyzed by X-ray diffractometer (XRD), energy disperse spectroscopy (EDS), etc.

## 2 Results and Discussion

### 2.1 Microstructure and phase analysis of $Al_3Zr$/Al matrix composites prepared in-situ

It can be seen from Fig.1 that the grain size of $Al_3Zr$/Al matrix composites prepared in-situ is about 50 μm, and the grain size of reinforcement phase $Al_3Zr$ is 5 μm, which is block or short bar, and distributed evenly. It can be seen from Fig.2 that the phase of $Al_3Zr$/Al matrix composites prepared in-situ is mainly composed of $Al_3Zr$ and a small amount of $Mg_2Si$ and Al phase.

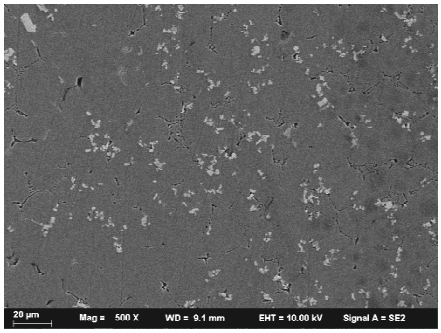


Fig.1 SEM image of $Al_3Zr$/aluminum matrix composites prepared in-situ

### 2.2 Microstructure and properties of $Al_3Zr$/Al matrix composites welded by plasma welding

#### 2.2.1 Microstructure of $Al_3Zr$/Al matrix composites and joints after plasma welding

It can be seen from Fig.3 that the Al-Ti-B at the weld seam forms a thin strip of compound phase after plasma arc welding with uniform size and uniform distribution. Combined with the XRD pattern of weld area in Fig.4, it can be seen that the whole composition of the phase contains the base metal and $Al_3Ti$, indicating that the $Al_3Ti$ phase is formed during welding, and the $Al_3Ti$ appears as a thin strip. In the welding process, through the heat input of 130 A, there is an imbalance of thermodynamic dynamics in the melting, cooling and solidifying process of the welding wire. This particular thermo-dynamic dynamic state leads to the formation of the $Al_3Ti$ phase. In order to reduce the resistance of phase transition, $Al_3Ti$ phase can easily grow into a fine strip[11,12]. This imbalance

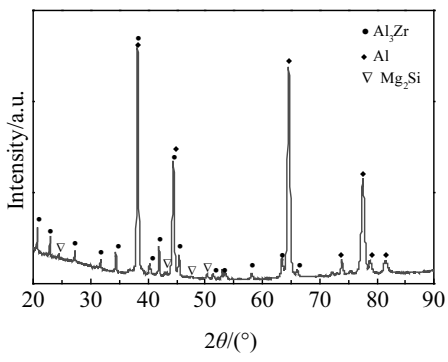


Fig.2 XRD pattern of $Al_3Zr$/aluminum matrix composites prepared in-situ

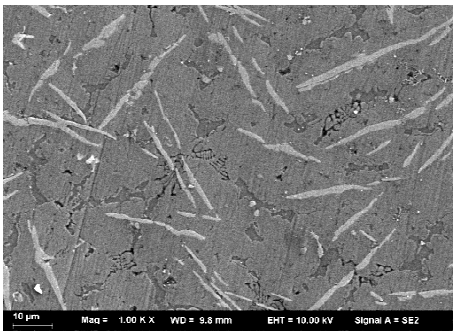


Fig.3 SEM image of weld area of $Al_3Zr$/aluminum matrix composites

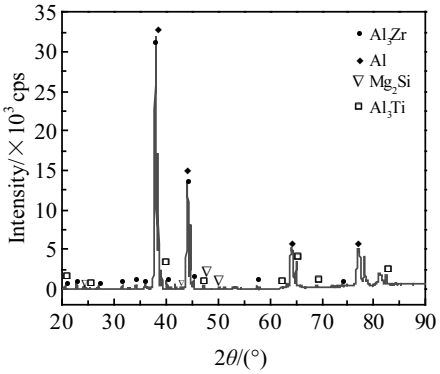


Fig.4 XRD pattern of weld area of $Al_3Zr$/aluminum matrix composites

will become less and less with the heat transfer between weld and base metal, which will promote the formation of $Al_3Ti$ near the heat-affected zone[13,14], and the Al, Ti element can fully diffuse and the $Al_3Ti$ phase can grow into approximately spherical shape. It can be seen from Fig.5 that the $Al_3Ti$ phase from weld fusion line to HAZ shows a common distribution of stripe and spheroid. Through EDS mapping in Fig.6, it can be seen that the weld and base metal are well fused, and the $Al_3Ti$ phase exhibits spherical distribution.

2.2.2 Microhardness testing and strengthening mechanism

Fig.7 shows the microhardness of base metal and weld area of $Al_3Zr$/aluminum matrix composites. It can be seen that the hardness of weld area, heat affected zone (HAZ) and base metal zone increases in turn. The hardness of base metal is the highest, and the hardness of weld area is the lowest, about 51% of the hardness of base metal. It can also be seen that when plasma welding $Al_3Zr$/aluminum matrix composites, the added Al-Ti-B can generate uniform distribution of $Al_3Ti$ after welding. It also has the function of refining the matrix grain, resulting in the second phase strengthening[15,16], which makes the welded joint excellent.

**2.3 Electrochemical comprehensive test results**

2.3.1 Electrochemical comprehensive tests and analysis of $Al_3Zr$/Al matrix composite and its weld

The Tafel polarization curves of $Al_3Zr$/aluminum matrix composites and their welds are shown in Fig.8. Fig.8 shows the polarization curves of the base metal of $Al_3Zr$/aluminum matrix composites and the weld nugget zone after plasma welding in 3.5% NaCl solution. It can be seen that the base metal shows the characteristics of anodic dissolution. Some researches show that in the early stage of soaking, the aluminum alloy is mainly anodized. The corrosion potentials of base metal and nugget are −720.76 and −847.01 mV, and corrosion current densities are $3.233\times10^{-6}$ and $4.5002\times10^{-6}$ A/cm$^2$ relative to the base metal, respectively.

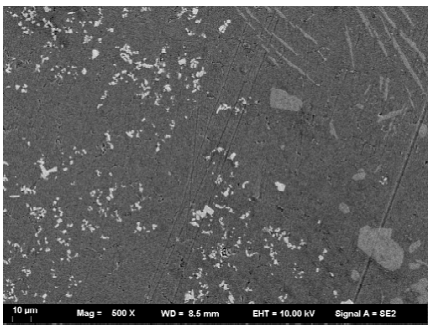


Fig.5 SEM image of welding heat affected zone and fusion line zone of $Al_3Zr$/aluminum matrix composites

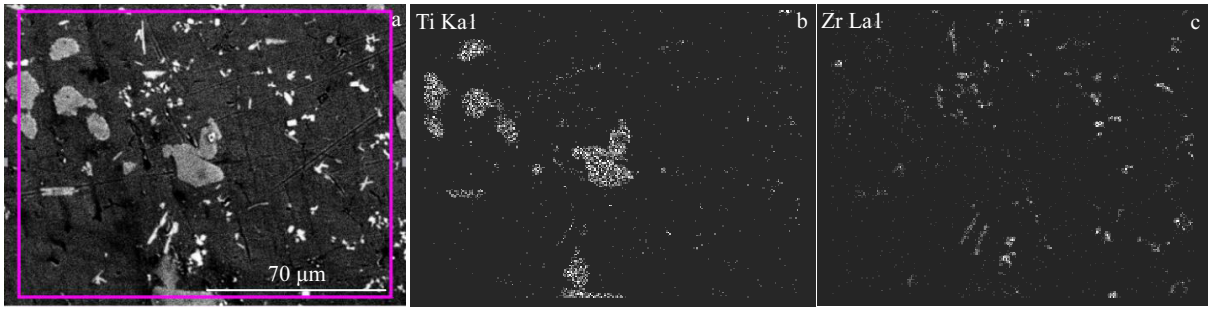


Fig.6 SEM image (a) of welding heat affected zone and fusion line zone of $Al_3Zr$/aluminum matrix composites; EDS mapping of Ti (b) and Zr (c) element

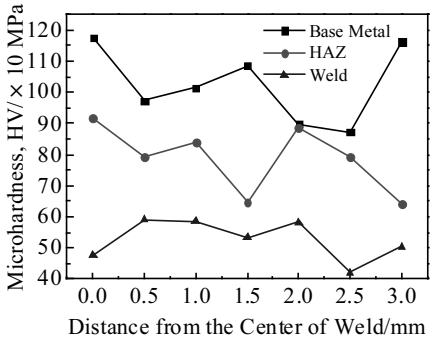


Fig.7 Microhardness of base metal and weld area of $Al_3Zr$/aluminum matrix composites

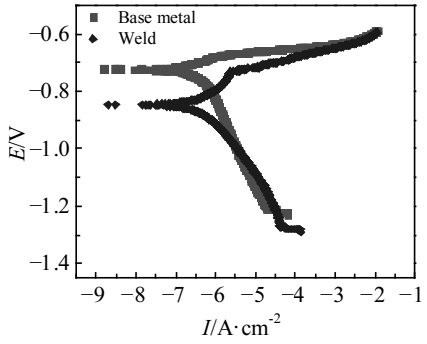


Fig.8 Polarization curves of base metal and weld area of $Al_3Zr$/aluminum matrix composites

The corrosion potential of the weld nugget zone decreases by 126.25 mV and the corrosion current density increases slightly. The results show that the corrosion resistance of the nugget is slightly lower than that of the base metal. This is because the high corrosion rate is due to a small amount of defective microstructure produced during welding[17,18].

2.3.2 Immersion experiment

The base metal of $Al_3Zr$/aluminum matrix composites immersed in 3.5% NaCl solution for 14 d was analyzed by EDS, as shown in Fig.9. It can be seen that the surface oxygen content of the composite is high after soaking. The EDS analysis results show that the content of O element is up to 43.11 wt%, which indicates that the $Al_3Zr$/aluminum matrix composites have been oxidized in brine.

The weld area of $Al_3Zr$/aluminum matrix composites after 14 d immersion was analyzed by EDS, as shown in Fig.10.

It can be seen that the oxygen content of the weld surface is higher, and the EDS analysis results show that the content of O element is 48.73 wt%, which indicates that the weld area is more seriously oxidized in brine. Combined with XRD analysis, it can be seen from Fig.11 that the phases in the weld area are mainly Al $(OH)_3$ and $Al_2O_3$[19-21]. The partial dissolution of the $Al_3Ti$ phase occurs during the soaking process, but the amount of surface $Al_3Ti$ phase decreases due to the dissolution, so $Al_3Ti$ phase is not obviously detected by XRD.

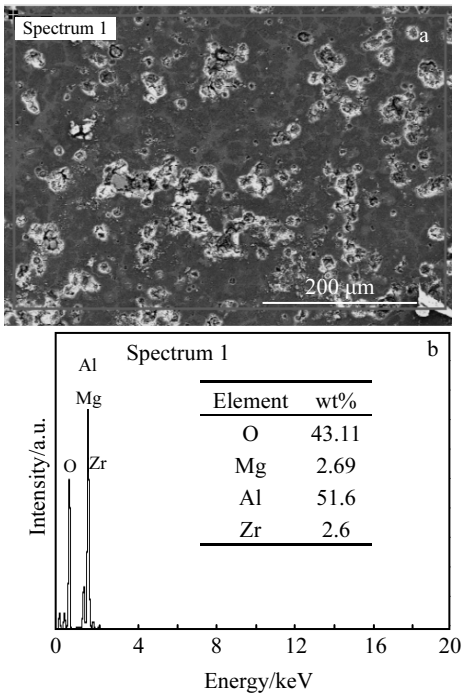


Fig.9 SEM image (a) and EDS results (b) of surface of $Al_3Zr$/aluminum matrix composites after immersion

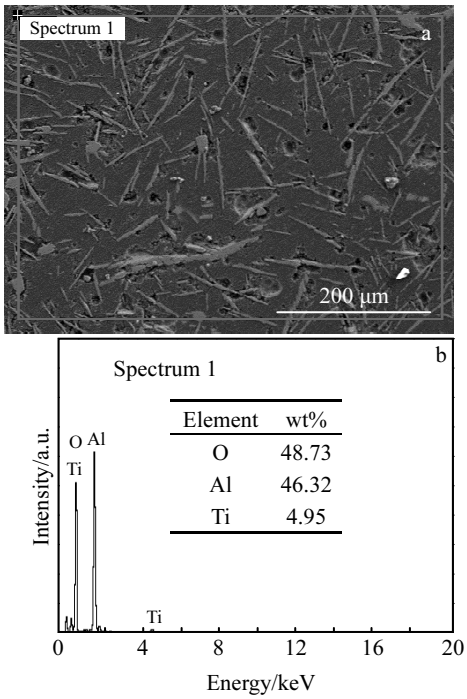


Fig.10 SEM image (a) and EDS results (b) of weld area after immersion

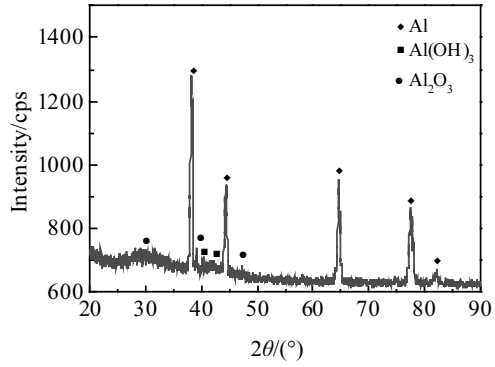


Fig.11 XRD pattern of weld area after immersion

2.3.3 Corrosion mechanism in weld area of $Al_3Zr$/Al matrix composites

The oxidation rate and corrosion rate of plasma welded joint samples are higher than those of base metal. The corrosion mechanism of plasma welded joints is analyzed as follows: according to the principle of electrochemical corrosion, in the corrosive medium containing conductive ion $Cl^-$, the main corrosion reason is electrochemical reaction, that is, electrochemical corrosion. Electrochemical corrosion occurs mainly at the interface, where the distribution of elements is more uneven than that of the matrix, and it is easier to induce the corrosion process including anodic reaction, cathode reaction or redox reaction. According to Gibbs free energy criterion, corrosion tendency is judged by electrode potential or standard electrode potential. The standard electrode potential of Al is −1.662V/Ti, and the standard electrode potential is −1.623 V/$Al_3Ti$/matrix primary battery. Corrosion is also the most likely to occur at the interface between the two cells at the beginning[22-24]. The corrosion trench between $Al_3Ti$ phase and matrix is also observed in the weld area, especially in the area with large $Al_3Ti$ reinforced particles; the corrosion degree is deeper, resulting in the $Al_3Ti$ particles to fall off, forming corrosion pits, and the number of Al3Ti phases on the surface decreases. As shown in Fig.12a, due to the high corrosion potential of the substrate, the $Al_3Ti$ phase acts as the cathode phase during the corrosion process, which leads to the corrosion of the surrounding matrix. In NaCl salt solution, the corrosion of aluminum is mainly oxygen absorption corrosion. The anodic reaction and the reduction of the cathode reaction to oxide are as follows[24,25]:

$$Al \rightarrow Al^{3+}+3e^- \quad (1)$$

$$O_2+4e^-+2H_2O \rightarrow 4OH^- \quad (2)$$

where $OH^-$ combines with $Al^{3+}$ to form $Al(OH)_3$, and the nodular corrosion product is formed with continuous deposition. In immersion corrosion tests, a dense $Al_2O_3$ corrosion product film is formed on the substrate, and the $Al_2O_3$ corrosion product film cracks along the grain boundary, as

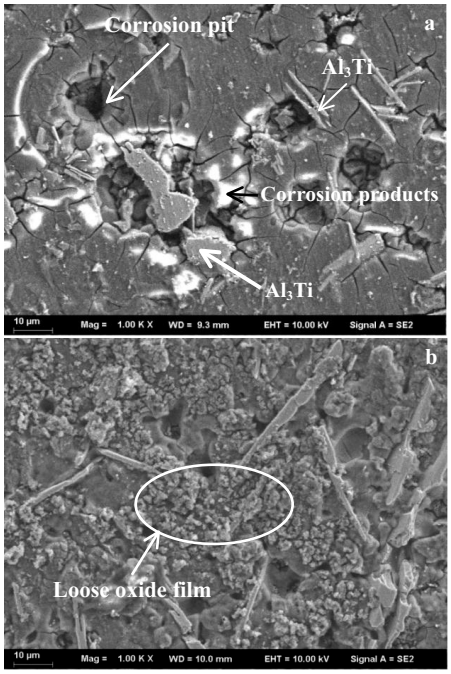


Fig.12 SEM images of corrosion pit (a) of $Al_3Zr$/aluminum matrix composite weld area and loose oxide film (b)

shown in Fig.12b. The following processes occur[24]:

$$Al+4Cl^- \rightarrow AlCl^-_4+3e^- \quad (3)$$

$$2AlCl_4+3H_2O \rightarrow Al_2O_3+8Cl^-+6H \quad (4)$$

$$2Al+3H_2O \rightarrow Al_2O_3+6H^++6e^- \quad (5)$$

## 3 Conclusions

1) Using 5 wt% $Al_3Zr$/aluminum matrix composite as base material and Al-Ti-B as welding wire material for plasma arc welding, a better weld can be obtained, and the $Al_3Ti$ phase in the weld is striped and spherical.

2) The electrochemical polarization curves show that the corrosion potential of base metal and nugget are −720.76 and −847.01 mV, respectively. The corrosion current densities are $3.233\times10^{-6}$ and $4.5002\times10^{-6}$ A/cm$^2$ relative to base metal, respectively. The corrosion potential of the weld nugget decreases by 126.25 mV, and the corrosion current density increases slightly, which indicates that the corrosion resistance of the materials at the nugget is slightly lower than that of the base metal.

3) After 14 d of soaking in 3.5% NaCl solution, the corrosion phase of weld is mainly composed of $Al(OH)_3$ and $Al_2O_3$. The corrosion mechanism is that the $Al_3Ti$ phase and the matrix phase behave as the anode and cathode of a primary cell, and the corrosion occurs at the interface between them, which results in the shedding and dissolving of the $Al_3Ti$ phase.

## References

1 Al-Fadhalah K J, Almazrouee A I, Aloraier A S. *Materials*

*Design*[J], 2014(53): 550
2 Xiao Bolu, Bi Jing, Zhao Mingjiu *et al*. *Acta Metallurgica Sinica* [J], 2002, 38(9): 1006
3 Jiao Lei, Zhao Yutao, Wu Yue *et al*. *Rare Metal Materials and Engineering*[J] , 2014, 43(1): 6
4 Chen Hongmei, Zang Qianhao, Yu Hui *et al*. *Materials Characterization*[J], 2015, 106: 437
5 Wang Zexin, Chen Guanqun, Chen Liangyu *et al*. *Metals*[J], 2018(8): 724
6 Vinod Kumar V Meti, Ramesh Konaraddi, Siddhalingeshwar I G *et al*. *Materials Today: Proceedings*[J], 2018(5): 25 677
7 Yang Yonggang, Zhao Yutao, Kai Xizhou *et al*. *Journal of Alloys and Compounds*[J], 2017, 710: 225
8 Xiang Hongfu, Dai Anlun, Wang Jiheng *et al*. *Transactions of Nonferrous Metals Society of China*[J], 2010, 20(11): 2174
9 Mahrle A, Schnick M, Rose S *et al*. *Journal of Physics D Applied Physics*[J], 2011, 44(34): 345
10 Chen S J, Yang X, Yu Y *et al*. *Weld Joining*[J], 2011(10): 1
11 Jiao Lei, Wang Xiaolu, Li Hui *et al*. *Rare Metal Materials and Engineering*[J], 2016, 45(11): 2798
12 Jiao Lei, Zhao Yutao, Chen Jianchao *et al*. *Rare Metal Materials and Engineering*[J], 2016, 35(12): 920
13 Szklarska-Smialowska Z. *Corrosion Science*[J], 1999, 41: 1743
14 Çam G, İpekoğlu G. *International Journal of Advanced Manufacturing Technology*[J], 2017, 91: 1851
15 Vairis A, Papazafeiropoulos G, Tsainis A M. *Advances in Manufacturing*[J], 2016(4): 296
16 Jiao Lei, Yang Yonggang, Li Hui *et al*. *Materials Research Express*[J], 2018, 5(5): 12
17 Li Hui, Jiao Lei, Mei Yunzhu *et al*. *Rare Metal Materials and Engineering*[J], 2017, 46(10): 3017
18 Zbigniew Szklarza, Halina Krawieca, Łukasz Rogal. *Materials Science & Engineering B*[J], 2019, 240: 23
19 Krawiec H, Szklarz Z. *Electrochimica Acta*[J], 2016, 203: 426
20 Dorin T, Stanford N, Birbilis N *et al*. *Corrosion Science*[J], 2015, 100: 396
21 Krawiec H, Szklarz Z, Vignal V. *Corrosion Science*[J], 2012, 65: 387
22 Guillaumin V, Mankowski G. *Corrosion Science*[J], 1998, 41(3): 421
23 Ferreira S C, Rocha L A, Ariza E *et al*. *Corrosion Science*[J], 2011, 53: 2058
24 Qiao Yanxin, Zhou Yang, Chen Shujin *et al*. *Acta Metallurgica Sinica*[J], 2016, 52(11): 1395
25 Pardo A, Merino M C, Merino S *et al*. *Corrosion Science*[J], 2005, 47: 1750

# 原位生成 $Al_3Zr$/Al 基复合材料等离子焊接组织及表面腐蚀行为

李　惠[1]，徐品一[1]，陆圣波[1]，焦　雷[2]
(1. 江苏科技大学，江苏 镇江 212003)
(2. 江苏大学，江苏 镇江 212013)

**摘　要**：以 5%$Al_3Zr$/铝基复合材料（质量分数）为研究对象，以 Ar 气体为离子气体，Al-Ti-B 为丝材进行等离子焊接。用电化学综合测试仪测定了焊接区在 3.5% NaCl 溶液中的腐蚀极化曲线。采用扫描电子显微镜（SEM）、X 射线衍射仪（XRD）对复合材料及其焊缝的组织和相组成进行了分析和表征，研究了 $Al_3Zr$/Al 基复合材料等离子焊接后在 3.5% NaCl 溶液中的腐蚀行为和腐蚀机理。SEM 分析结果表明，等离子弧焊接可获得较好的焊缝组织，焊缝组织主要由 $Al_3Ti$ 相和 Al 基体组成，$Al_3Ti$ 相呈条状和球形。电化学极化曲线表明，材料在熔核处的耐蚀性略低于母材，焊缝处浸泡腐蚀机理为 $Al_3Ti$ 相和基体相的电极电位不同形成原电池反应。

**关键词**：原位生成 $Al_3Zr$/Al 基复合材料；等离子弧焊；耐蚀性；腐蚀机理

作者简介：李　惠，女，1979 年生，博士，副教授，江苏科技大学材料科学与工程学院，江苏 镇江 212003，电话：0511-84426291，E-mail: lihuiwind@163.com